JOURNAL OF APPLIED ELECTROCHEMISTRY **28** (1998) 387–396

A wall-jet electrode reactor and its application to the study of electrode reaction mechanisms Part III: Study of the mechanism of the a.c. electrolytic graining of aluminium in hydrochloric acid

P. LAEVERS

Monroe Europe N.V., I.Z. A Schurhovenveld 1420, 3800 Sint-Truiden, Belgium

A. HUBIN, H. TERRYN, J. VEREECKEN

Department of Metallurgy, Electrochemistry and Materials Science, Vrije Universiteit Brussel, Pleinlaan 2, 1050 Brussels, Belgium

Received 24 August 1996; revised 9 April 1997

The mechanism of the a.c. electrolytic graining of aluminium in hydrochloric acid is determined from the analysis of the potentiostatic transient behaviour of the system aluminium–electrolyte under anodic and cathodic polarization and comparison of experimentally determined transients with calculated values derived from a candidate mechanistic scheme. It has been established, that the oxidation of aluminium in the development of a distinct surface morphology occurs according to

$$Al + 3\,Cl^- \xrightarrow{k_1} Al(Cl)_3 + 3\,e^-$$

$$Al(Cl)_3 \xrightarrow{k_2} Al^{3+} + 3\,Cl^-$$

the Al^{3+} ions being dissolved from the surface and removed to the bulk of the solution, hence forming pits. $Al(Cl)_3$ is a solid intermediate. The morphology developed, is determined by the excess of Cl^- ions created at the electrode surface, with respect to the bulk concentration. The accumulation of Cl^- ions is governed by the ratio between the rate constant for the formation of $Al(Cl)_3$, set by the flux of charges forced across the electrode–solution interface per unit surface area taking part in the active dissolution of aluminium and the mass transport rate of the Cl^- ions. The reduction of H^+ ions in the cathodic half period of the applied alternating current is mass transport controlled. The concomitant rise in interfacial pH causes Al^{3+} ions formed in the preceding anodic half period, which are not yet removed from the electrode–solution interface, to precipitate as aluminium.

Keywords: *aluminium oxidation, electrolytic graining, reaction mechanisms, wall-jet electrode reactor*

List of symbols

A	active surface area $(m)^2$
C	capacitance of the electrode–solution interface (F)
C_{dl}	double layer capacitance (F)
C_{etch}	capacitance of the layer of etch products (F)
$C_{i,j}$	concentration of i in the elementary step j (mol m^{-3})
$\underline{C}_i$	normalized concentration of i (mol m^{-3})
C_i^{bulk}	concentration of i in the bulk (mol m^{-3})
d	thickness of the layer of etch products (m)
D_i	diffusion coefficient of i ($m^2\,s^{-1}$)
DN_1, DN_2	dimensionless numbers expressing the relative magnitude of the formation and dissolution rate of $Al(Cl)_3$ to the mass transport rate of Cl^- ions
E	applied potential (V)
E_{gr}	open circuit potential taken by the grained substrate at the end of the 1 s deadtime (V)
E_{gr}^m	arithmetic mean of ten measured values of E_{gr} (V)
F	faradaic constant (C)
I	electrode current (A)
$I_{DN_1 \ll 1}^{ss}$	steady state current for $DN_1 \ll 1$ (A)
J	current density ($A_{rms}\,m^{-2}$)
k_1, k_2	reaction rate constants $I_{DN_1 \ll 1}^{ss}$
k_j^f, k_j^b	forward and backward rate constant of the elementary step j
M	flux of exterior momentum flux ($m^7\,s^{-3}$)
R	radius of the working electrode (m)
R_{el}	ohmic resistance of the electrolyte (Ω)
R_{etch}	ohmic resistance of the layer of etch products (Ω)
R_tI	ohmic voltage drop (V)

0021-891X

S	electrode surface area (m^2)
t	time (s)
t_d	deadtime (s)
t_{gr}	graining time (s)
V	potential available at the electrode surface (V)
V_f	volume flow rate ($m^3\,s^{-1}$)

Greek letters

ε	relative permeability
ε_0	permeability of vacuum ($F\,m^{-1}$)
κ	specific conductance ($\Omega^{-1}\,m^{-1}$)
ν	kinematic viscosity ($m^2\,s^{-1}$)
η	dimensionless distance normal to the impinged electrode
ξ	dimensionless distance along the impinged electrode
τ	dimensionless time

1. Introduction

Producing aluminium lithographic plates for offset printing involves roughening or graining of the aluminium base to increase the surface area, which is necessary to improve the adhesion of the photosensitive coating and to enhance the water retentive properties of the aluminium surface. The parts of the photosensitive coating remaining on the aluminium base after development constitute the printing image of the lithographic plate. The revealed parts of the aluminium surface constitute the water retaining non-image areas. Hence, the roughening of the aluminium surface conspicuously affects the printability and durability of the plate. The quality of the graining or surface morphology is therefore one of the most important factors in producing effective aluminium lithographic printing plates.

The roughening of the aluminium base for lithographic plates is most commonly carried out by a.c. electrolytic graining or electrograining. This surface treatment is a highly controlled electrochemically induced pitting process, involving the application of an alternating current on the aluminium substrate in a suitable electrolyte (e.g., hydrochloric acid). Under the alternating current, pitting and aluminium dissolution occur during the anodic half period, while reduction of protons during the cathodic half period and the concomitant rise in interfacial pH, provoke the formation of a passivating film, resulting in a redistribution of attack during the subsequent anodic half period. The resultant a.c. electrolytic graining morphology is determined by the particular electrical, electrolyte and substrate conditions used [1–7], as illustrated in Fig. 1.

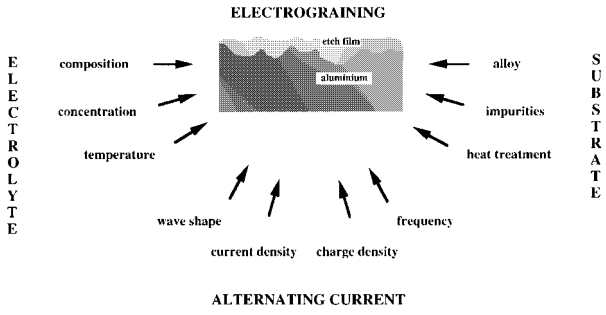

Fig. 1. Process parameters of the a.c. electrolytic graining of aluminium.

The development of a distinct morphology is correlated with the ratio between the number of sites where key pits are initiated and the development rate of the sites [7]. The number of sites where morphological building elements are due to initiate and the susceptibility of the sites for pit initiation is determined by the surface condition of the aluminium substrate [5–7]. The activation of the sites depends upon the electrolyte conditions [1, 4, 7]. The propagation rate of the sites is dependent upon the features of the applied alternating current and the proportion of the current concentrated at the pit site [2, 5, 7].

For treatment in hydrochloric acid, the combined action of repeated initiation, propagation and repassivation of pits results in the formation of three characteristic a.c. electrolytic graining morphologies: a nonuniform and uniform morphology characterized by hemispherical pits, their walls decorated with a high population density of key cubic pits and an etched-like morphology, comprised of an abundant number of uniformly distributed cubic pits. The features distinguishing the characteristic nonuniform and uniform morphology are the average size and the population density of the hemispherical pits [5–7]. In Fig. 2 the characteristic morphologies are arranged in a current density–concentration diagram [7]. The key cubic pit building them up, is shown in Fig. 3 [5, 7].

In this paper, a quantitative electrochemical investigation of the mechanism of the electrode processes involved in the a.c. electrolytic graining of aluminium in hydrochloric acid is reported. The investigation includes potential step experiments in a dedicated wall-jet electrode reactor, to examine the role of mass transport in the overall kinetics of the electrode processes and comparison of experimentally determined current transients with calculated values derived, from candidate mechanistic schemes. The design and construction of the dedicated wall-jet electrode reactor, as well as the numerical computational method developed to solve the mass transport problems involved in using a wall-jet electrode reactor as a hydrodynamic electrode system in a quantitative investigation of electrode reaction mechanisms, were reported [8, 9]. The wall-jet electrode reactor is characterized by the size of the impinged electrode surface and is designed to suit the need for a large working electrode surface area, such as in the study of the mechanism of the a.c. electrolytic graining of rolled aluminium [8]. The computational method is

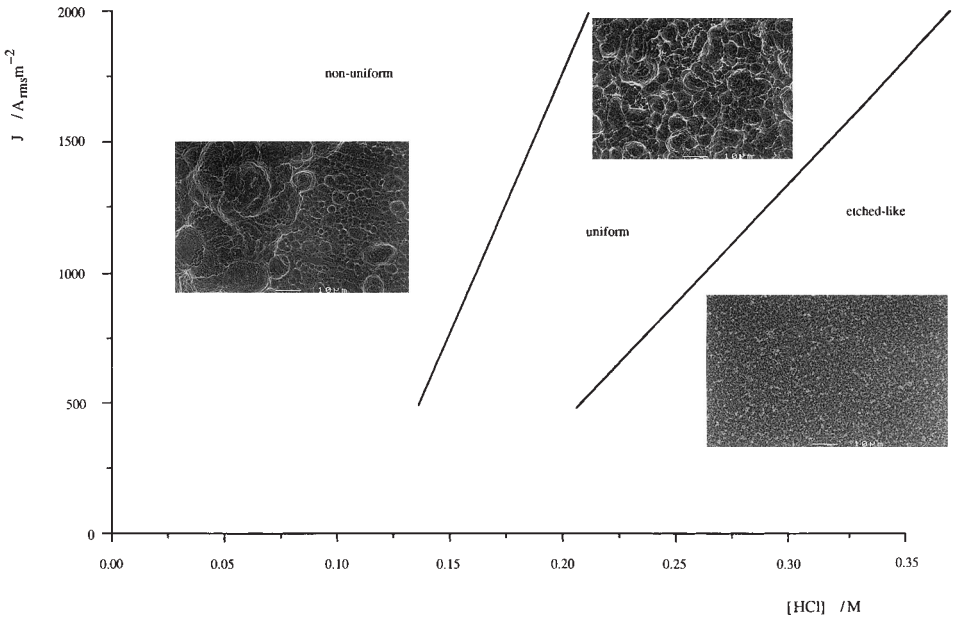

Fig. 2. Current density–concentration diagram, showing the characteristic a.c. electrolytic graining morphologies obtained in hydrochloric acid [7].

based on a second order-correct implicit, finite difference approach, and a space coordinate transformation making the use of a simple Cartesian grid compatible with efficient computing [9].

2. Experimental details

The a.c. electrolytic graining experiments were carried out in a dedicated wall-jet electrode reactor. All detailed information concerning the design, construction and evaluation of the reactor was reported earlier [8]. The surface area of the working electrode was set by an electrode holder having an opening of 20.00 mm in radius. The distance between the tip of the nozzle and the working electrode was 26 mm. The nozzle diameter equalled 200 mm. The volume flow rate was varied between 1.7×10^{-6} and $4.3 \times 10^{-6}\,m^3\,s^{-1}$. The counter electrode was a 5 mm thick disc produced from a rod of 99.99% pure aluminium. A saturated calomel reference electrode was used. A Tacussel 20-50X potentiostat, combined with a Wavetek 75 wave form generator, was used to apply a sinusoidal alternating current of frequency 50 Hz. The electrolytic solutions worked in, were a 0.20, 0.25 and 0.30 M hydrochloric acid solution, the substrates being grained with a current density of $1 \times 10^3\,A_{rms}\,m^{-2}$. The applied charge density was $3 \times 10^5\,C\,m^{-2}$. The substrates were produced from 99.99% purity aluminium sheet material.

The chronoamperometric transient measurements were carried out using a Solartron electrochemical interface 1186, combined with an Amel 567 function generator. The current transients were recorded on a Nicolet 310 oscilloscope. The processing of the data was performed on an IBM personal computer, equipped with the commercially available signal analysis package, FAMOS of Integrated Measurement & Control. Before a.c. electrolytic graining, the sheet specimens were degreased with a weak alkaline cleaner and rinsed with deionized water. The degreasing and graining solutions were all made up from proanalysis reagents and deionized water. All experiments were carried out under thermostatic conditions at $25 \pm 0.5\,^{\circ}C$.

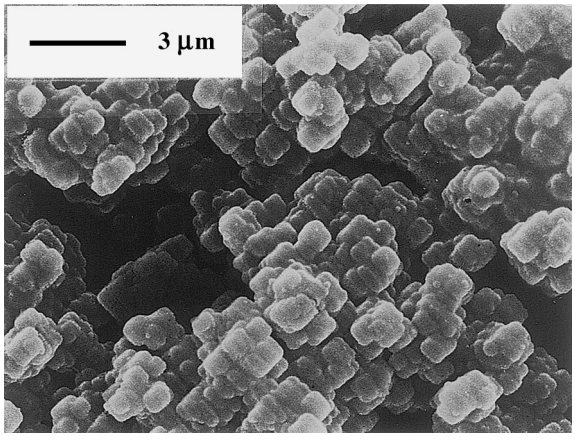

Fig. 3. Key cubic pit building up the characteristic a.c. electrolytic graining morphologies obtained in hydrochloric acid [5, 7].

3. Results and discussion

3.1. *Analysis of the potentiostatic transient behaviour*

The mechanism of the a.c. electrolytic graining of aluminium is determined from the analysis of the potentiostatic transient behaviour of the system aluminium–electrolyte under anodic and cathodic polarization and comparison of experimentally determined transients with calculated ones derived from a candidate mechanistic scheme. For the potentiostatic transient behaviour under anodic and

cathodic polarization to be representative of the electrochemical behaviour of the system aluminium–electrolyte during the a.c. electrolytic graining, the chronoamperometric transients are recorded *in situ*, subsequent to the interruption of the graining process. As an example, the recording of the current transients under anodic polarization is schematically illustrated in Fig. 4. E_{gr} is the open circuit potential taken by the grained substrate at the end of the deadtime t_d. The potential is stepped anodically or cathodically with respect to E_{gr}. To avoid difficulties originating from fluctuations in E_{gr}, the transient measurements are performed, only if

$$E_{gr} = E_{gr}^{m} \pm 5\,\text{mV} \qquad (1)$$

where E_{gr}^{m} is the arithmetic mean of ten measured values, determined up front for each experiment. The graining time t_{gr} is set for an applied charge density of $3 \times 10^5\,\text{C m}^{-2}$. The dead time is set constant at 1 s. This is the minimal dead time necessary to avoid problems arising from the interaction of apparatus. Ideally, the deadtime is zero.

Preliminary graining experiments in the wall-jet electrode reactor revealed that the diagonal lines separating the morphological characteristic regions in the current density–concentration diagram, shift to lower hydrochloric acid concentration with increasing volume flow rate, as illustrated in Figs 5–8.

The influence of convection is most explicit for treatment with a combination of current density and hydrochloric acid concentration left of, and close to, the diagonal line separating the regions of uniform and etched-like morphology. Such a combination gives rise to the uniform morphology at low volume flow rate, while resulting in the etched-like morphology at high volume flow rate.

The frame of investigation for the analysis of the potentiostatic transient behaviour is therefore set across the boundary region between the morphological characteristic uniform and etched-like regions. The electrolytic solutions worked in, are a 0.20, 0.25 and 0.30 M hydrochloric acid solution. At low volume flow rate ($1.7 \times 10^{-6}\,\text{m}^3\,\text{s}^{-1}$), surfaces treated in the 0.25 M hydrochloric acid solution exhibit the characteristic uniform morphology, yet at high volume flow rate ($4.3 \times 10^{-6}\,\text{m}^3\,\text{s}^{-1}$), the etched-like morphology is obtained. In the 0.20 and 0.30 M hydrochloric acid solution the uniform and etched-like morphology are obtained, respectively, at either volume flow rate.

E_{gr}^{m} is determined to be $-760, -755$ and -755 mV vs SCE $\pm$ 15 mV for treatment in the 0.20, 0.25 and 0.30 M hydrochloric acid solution, respectively.

3.2. *Anodic polarization*

3.2.1. The transient current response. Figures 5–8 show the transient current response of the system aluminium–electrolyte subsequent to a.c. electrolytic graining in 0.20, 0.25 and 0.30 M hydrochloric acid solution at low and high volume flow rate, the

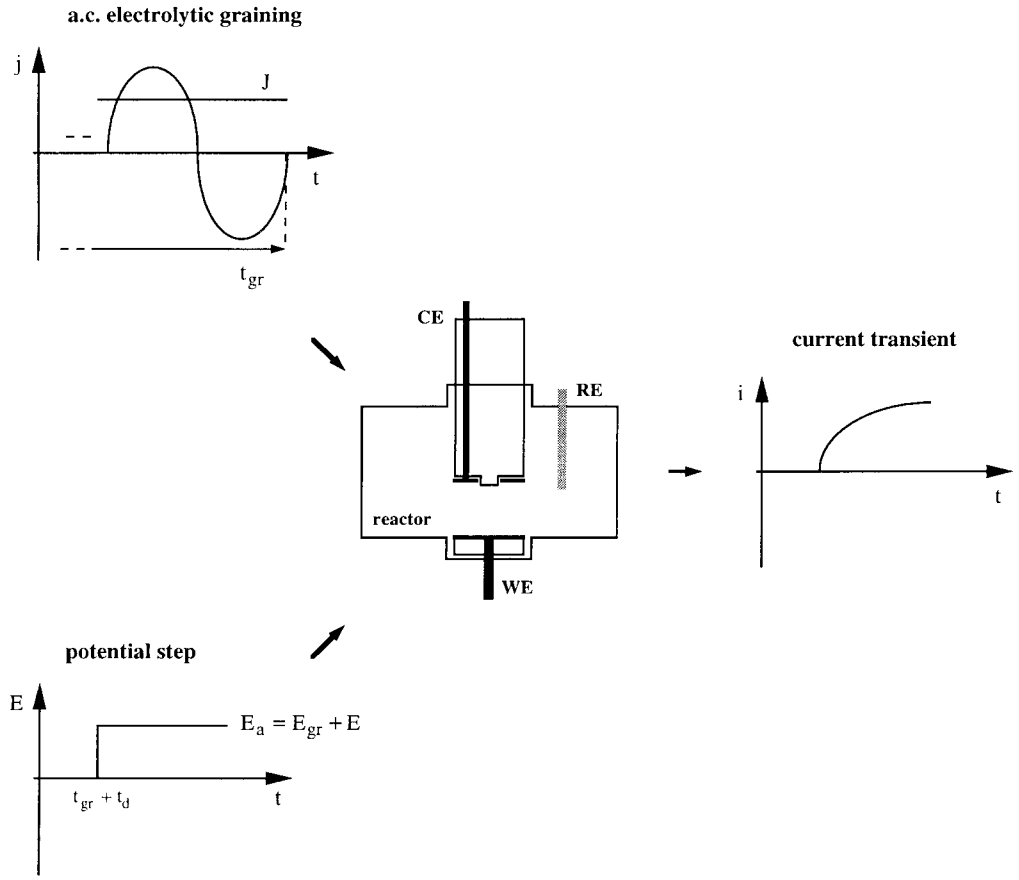

Fig. 4. Recording of the chronoamperometric transients, e.g. under anodic polarization.

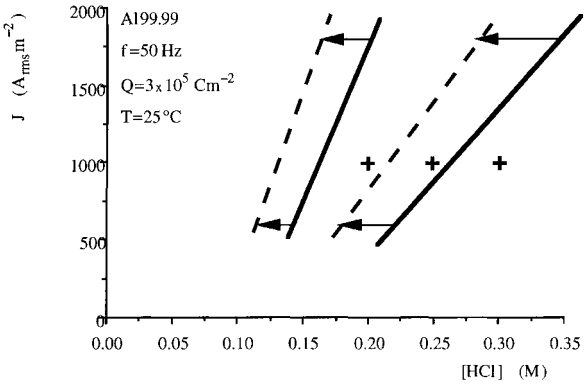

Fig. 5. Current density–concentration diagram. Key: (——) $V_f = 1.7 \times 10^{-6}\ m^3\ s^{-1}$; (- - - -) $V_f = 4.3 \times 10^{-6}\ m^3\ s^{-1}$.

potential being stepped 100, 150 and 200 mV anodically of E_{gr}.

Although exhibiting some fluctuations, the relative magnitude of which do not exceed 2% of the corresponding geometrical mean, the chronoamperometric transients are well defined, increasing from zero to a steady state current in seconds. The reproducibility of the transients is illustrated in Fig. 9, for the current response in the 0.25 M solution at either low or high volume flow rate, the potential being stepped anodically by 150 mV. As can be seen, the three transients reported for each experiment practically coincide. The currents at any instant disagree, at the worst, by 3 to 5% .

From Figs 5–8 it is evident that in all three hydrochloric acid solutions the transient current response is strongly affected by the level of polarization. At low, as well as high, volume flow rate the steady state current increases quasi linearly with increasing polarization, the time necessary to attain the steady state current being decreased. The transient current response in the 0.20 M hydrochloric acid solution is independent of the volume flow rate. Conversely, the potentiostatic transient behaviour of the system aluminium–electrolyte in the 0.30 M hydrochloric acid solution exhibits a clear dependency

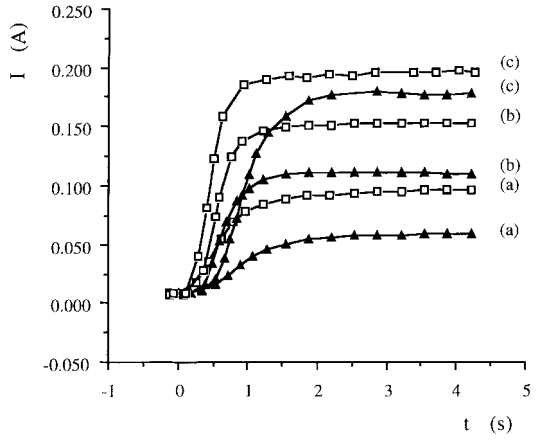

Fig. 7. Anodic potentiostatic transient behaviour, [HCl] = 0.25 M. $E - E_{gr}$: as for Fig. 6; Key: as for Fig. 6.

on the volume flow rate, an increase in volume flow rate causing the steady state current to decrease. The dependence is most clearly pronounced at higher polarization. In the 0.25 M hydrochloric acid solution, the transient current responses at low and high volume flow rate being similar in shape to those obtained in 0.20 and 0.30 M hydrochloric acid, respectively, indicates that here the apparent dependence on the volume flow rate is probably correlated to the change in a.c. electrolytic graining morphology. At low volume flow rate, surfaces treated in the 0.25 M hydrochloric acid solution exhibit the uniform morphology, whereas at high volume flow rate, an etched-like morphology is obtained. In the 0.20 and 0.30 M hydrochloric acid solution the uniform and etched-like morphology are obtained, respectively, at low as well as at high volume flow rate.

It is thus apparent, that the transient current response following the development of the etched-like morphology is a function both of the applied potential and the volume flow rate, whereas the transient current response subsequent to the development of the uniform morphology is only a function of the applied potential. However, a difference occurs in the steady state current attained following the develop-

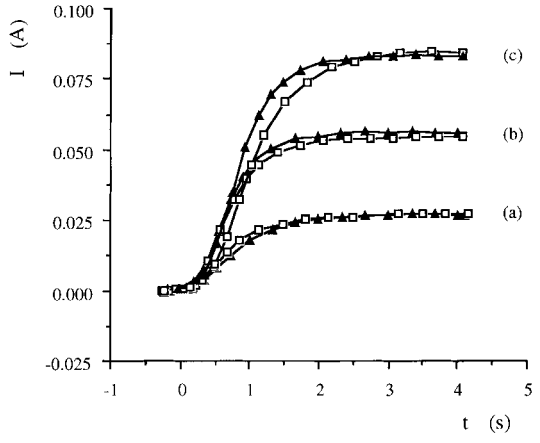

Fig. 6. Anodic potentiostatic transient behaviour, [HCl] = 0.20 M. $E - E_{gr}$: (a) 100, (b) 150 and (c) 200 mV. Key: (▲) $V_f = 1.7 \times 10^{-6}\ m^3\ s^{-1}$; (□) $V_f = 4.3 \times 10^{-6}\ m^3\ s^{-1}$.

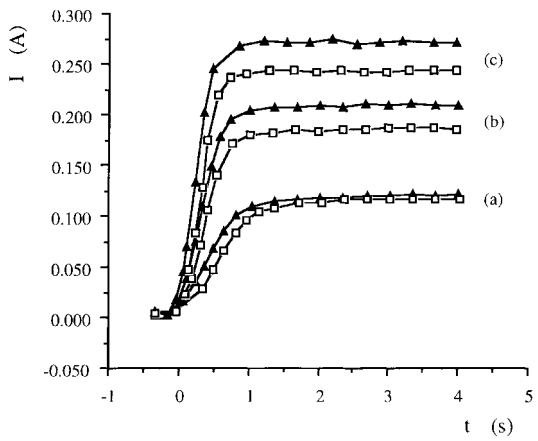

Fig. 8. Anodic potentiostatic transient behaviour, [HCl] = 0.30 M $E - E_{gr}$: as for Fig. 6; Key: as for Fig. 6.

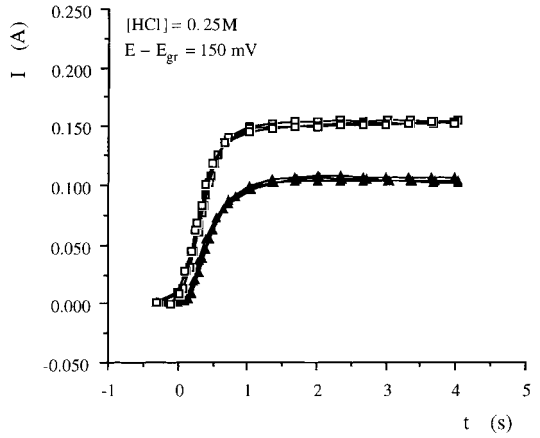

Fig. 9. Typical example of the reproducibility of the anodic transient current response. V_f: (▲) $1.7 \times 10^{-6}\,m^3\,s^{-1}$; (□) $4.3 \times 10^{-6}\,m^3\,s^{-1}$.

ment of the etched-like and uniform morphology for a given polarization, the steady state currents being in proportion by between 2 and 4 to 1, respectively.

3.2.2. A candidate mechanistic scheme: computation of the transient current response. The transient current response of the system aluminium–electrolyte following the a.c. electrolytic graining is determined by the rate of the oxidation of aluminium in the development of the distinct surface morphology on one hand and the capacitance of the electrode–solution interface on the other.

The transient current is thus given by

$$\frac{I}{A} = f\left(I_f((k_j^f, k_j^b, C_{i,j})_{Al^{3+}}, V) + I_c(C, E), A\right) \qquad (2)$$

The first term in the sum of currents on the right-hand-side of Equation 2, the faradaic current, is function of the kinetics of the elementary steps involved in the oxidation of aluminium. The second term is the capacitive current, due to charging of the electrode–solution interface. The potential available for the oxidation of aluminium is related to the applied potential, that is,

$$V = E - R_t I = E - (R_{etch} + R_{el})I \qquad (3)$$

where R_tI, the ohmic drop, accounts for the voltage drop across the layer of etch products developed over the aluminium surface ($R_{etch}I$) and the solution voltage drop ($R_{el}I$).

Taking into account Equation 3, Equation 2 takes the form

$$\frac{I}{A} = f\left(I_f((k_j^f, k_j^b, C_{i,j})_{Al^{3+}}, E, R_t) + I_c(C, E), A\right) \qquad (4)$$

The capacitive current decays approximately exponentially with time [10]

$$I_c \approx \frac{E}{R_{el}} \exp\left(\frac{-t}{R_{el}C}\right) \qquad (5)$$

The current due to charging of the electrode–solution interface capacitance will drop to 5% of its initial value (E/R_{el}) at $t = 3 \times (R_{el}C)$. Representative values for R_{el} and C are estimated to be $1\,\Omega$ and $1 \times 10^{-5}\,F$, respectively. The ohmic resistance is calculated from [11]

$$R_{el} = \frac{1}{4\kappa R} \qquad (6)$$

The capacitance of the electrode solution interface, determined by double layer effects and the capacitive effect of the layer of etch products developed over the aluminium surface during the a.c. electrolytic graining, is calculated from [10, 12]

$$C = \left(\frac{1}{C_{etch}} + \frac{1}{C_{dl}}\right)^{-1} = \left(\frac{d}{\varepsilon\varepsilon_0 S} + \frac{1}{C_{dl}}\right)^{-1} \qquad (7)$$

The layer of etch products is considered to be a dielectric aluminium hydroxide film, the thickness of which is estimated from the weight of the etch layer developed over the electrode surface.

The charging of the electrode–solution interface is thus estimated to be completed in tens of microseconds. Hence, given the time scale of seconds for the system aluminium–electrolyte to regain a steady state upon the potential step perturbation, the contribution of charging of the electrode–solution interface capacitance to the transient current may be disregarded. Equation 4 thus reduces to

$$I = f\left(I_f((k_j^f, k_j^b, C_{i,j})_{Al^{3+}}, E, R_t), A\right) \times A \qquad (8)$$

Differences in transient current response subsequent to the development of the uniform and etched-like morphology are thus due either to the ohmic voltage drop, provoking a change in the potential available for the oxidation of aluminium and therefore in the rate and possibly in the elementary step governing the electrochemical reaction, or to the active surface area being different, or both.

However, if the differences in transient current response were solely due to the active surface area being different, there would be no reason for the transient current response to be dependent upon the volume flow rate following the development of the etched-like morphology and not to be affected by the volume flow rate subsequent to the development of the uniform morphology.

From the work of Richardson *et al.* [15–17], in which pitting is postulated as the active dissolution of bare metal in defects of the protecting oxide layer under attack by aggressive anions, the mechanism for the oxidation of aluminium by the participation of chloride ions is suggested to be

$$\begin{aligned} Al + 3\,Cl^- &\xrightarrow{k_1} Al(Cl)_3 + 3\,e^- \\ Al(Cl)_3 &\xrightarrow{k_2} Al^{3+} + 3\,Cl^- \end{aligned} \qquad (9)$$

It is assumed that the Al^{3+} ion is the only soluble reaction product and that the formation of $Al(Cl)_3$ is rate determining, meaning that it does not develop into an aluminium chloride film. The rate constant k_1 is representative for the combination of charge transfer and heterogeneous chemical reactions which lead to the formation of the $Al(Cl)_3$. Therefore, k_1 is

constant at constant potential available for the oxidation of aluminium. The k_2 is a chemical rate constant, determining the dissolution rate of the $Al(Cl)_3$.

Calculating chronoamperometric transients for the above scheme of successive reactions at the impinged surface of the wall-jet electrode reactor requires the mass transport problem in the reactor to be solved for a multicomponent electrochemical system involving the ionic species Al^{3+}, H^+ and Cl^- and the solvent water, which is a complex problem. It was, however, established [11, 18], that a good approximation can be achieved from a computation based on the convective diffusion equation using effective or integral diffusion coefficients. The convective diffusion equation is strictly valid only in the two limiting cases of a binary electrolyte solution on one hand and a minor electroactive species in a solution with an excess of indifferent electrolyte on the other [11, 18].

The convective diffusion equations and boundary for the relevant species at the impinged surface of the wall-jet electrode reactor are expressed in the dimensionless computational (ξ, η, τ)-space, introduced in the second paper of this series on the numerical computational method developed to solve the mass transport problems involved in using the wall-jet electrode reactor as a hydrodynamic electrode system [9]:

$$\xi^{5/2}\frac{\partial \underline{C}_{Al^{3+}}}{\partial \tau} = \frac{D_{Al^{3+}}}{D_{Cl^-}}\frac{\partial^2 \underline{C}_{Al^{3+}}}{\partial \eta^2} - \frac{8v}{27 D_{Cl^-}} \times \xi\eta\,\frac{\partial \underline{C}_{Al^{3+}}}{\partial \xi} + \frac{v}{9D_{Cl^-}}\,\eta^2\frac{\partial \underline{C}_{Al^{3+}}}{\partial \eta} \tag{10}$$

$$\xi^{5/2}\frac{\partial \underline{C}_{Cl^-}}{\partial \tau} = \frac{\partial^2 \underline{C}_{Cl^-}}{\partial \eta^2} - \frac{8v}{27 D_{Cl^-}} \times \xi\eta\,\frac{\partial \underline{C}_{Cl^-}}{\partial \xi} + \frac{v}{9D_{Cl^-}}\,\eta^2\frac{\partial \underline{C}_{Cl^-}}{\partial \eta} \tag{11}$$

$$\tau \le 0 \quad 0 \le \xi \le 1 \quad 0 \le \eta \le \eta_c$$
$$\underline{C}_{Al^{3+}} = 0$$
$$\underline{C}_{Cl^-} = 1 \tag{12}$$

$$\tau > 0 \quad 0 \le \xi \le 1 \quad \eta = 0$$
$$\frac{\partial \underline{C}_{Al^{3+}}}{\partial \eta} = -DN_1\,\frac{D_{Cl^-}}{D_{Al^{3+}}}\,\underline{C}^3_{Cl^-}\,\xi^{5/4}$$
$$\frac{\partial \underline{C}_{Cl^-}}{\partial \eta} = 3\left(DN_1\,\underline{C}^3_{Cl^-} - DN_2\right)\,\xi^{5/4} \tag{13}$$

$$0 \le \xi \le 1 \quad \eta = \eta_c$$
$$\underline{C}_{Al^{3+}} = 0$$
$$\underline{C}_{Cl^-} = 1 \tag{14}$$

$$\xi = 0 \quad 0 < \eta \le \eta_c$$
$$\underline{C}_{Al^{3+}} = 0 \qquad \underline{C}_{Cl^-} = 1$$
$$\frac{\partial \underline{C}_{Al^{3+}}}{\partial \xi} = 0 \qquad \frac{\partial \underline{C}_{Cl^-}}{\partial \xi} = 0 \tag{15}$$

where

$$\underline{C}_{Al^{3+}} = \frac{C_{Al^{3+}}}{C^{bulk}_{Cl^-}} \quad \text{and} \quad \underline{C}_{Cl^-} = \frac{C_{Cl^-}}{C^{bulk}_{Cl^-}} \tag{16}$$

are the concentrations of the Al^{3+} and Cl^- ions, respectively, referred to the bulk concentration of the chloride ions. The dimensionless numbers

$$DN_1 = \frac{k_1\left(C^{bulk}_{Cl^-}\right)^3}{D_{Cl^-}\left(\frac{135M}{32\nu^3R^5}\right)^{1/4} C^{bulk}_{Cl^-}} \tag{17}$$

$$DN_2 = \frac{k_2}{D_{Cl^-}\left(\frac{135M}{32\nu^3R^5}\right)^{1/4} C^{bulk}_{Cl^-}} \tag{18}$$

are a measure of the relative magnitude of the formation and dissolution rate of $Al(Cl)_3$ to the mass transport rate of Cl^- ions, respectively.

The dimensionless time is related to the species with the largest effective diffusion coefficient, that is, the chloride ions, in order to obtain maximum stability and accuracy for the calculations [19]. The effective diffusion coefficients of Cl^- and Al^{3+} are estimated to be in proportion to one another as the diffusion coefficients of both ions in ideal dilute solutions, that is in proportion of 2 to 1 [7]. The boundary conditions at the impinged surface are determined by the assumption that $Al(Cl)_3$ does not develop into an aluminium chloride film, that is $k_2 > k_1\underline{C}^3_{Cl^-}$.

There is a nonlinear boundary condition arising from the cubic dependency on the chloride ion concentration of the formation rate of $Al(Cl)_3$. The transient current is determined from [9]

$$I = -\int_0^1 3F\,D_{Al^{3+}}\,C^{bulk}_{Cl^-}\,\xi^{-1/4}\left(2\pi R^{3/4}\right) \times \left(\frac{135M}{32\nu^3}\right)^{1/4}\left(\frac{\partial \underline{C}_{Al^{3+}}}{\partial \eta}\right)_{\eta=0} d\xi \tag{19}$$

It must be emphasized that in this model the rather difficult geometry of the aluminium surface is not considered, that is, the impinged electrode surface is approximated to be planar. Moreover, the active surface area is taken to be equal to the impinged surface area.

It is evident, that the calculation of the numerical value of the concentration profiles and hence of the transient current for a given level of polarization and volume flow rate, requires the knowledge of the effective diffusion coefficients of Al^{3+} and Cl^- in the electrochemical system at hand and of the rate constants k_1 and k_2, neither of which are available or can *a priori* be determined by independent means. However, by calculating the concentration profiles of Al^{3+} and Cl^- for the limiting cases in which the formation and dissolution of $Al(Cl)_3$ are either mass transport or reaction controlled, the dependency of the current transient on the applied potential and the volume flow rate can be determined. Taking into account the assumption that $Al(Cl)_3$ does not develop into an aluminium chloride film ($k_2 > k_1\underline{C}^3_{Cl^-}$) and that mass transport has been shown to be involved in the oxi-

dation of aluminium, the cases to be considered correspond to

$$DN_2 \gg 1 \quad \text{with} \quad DN_1 \approx 1 \quad \text{or} \quad DN_1 \ll 1 \qquad (20)$$

The above set of partial differential equations, together with the appropriate boundary conditions, is solved using the space and equation discretization outlined earlier [9]. The method for handling the nonlinear boundary condition of Equation 13 is based on a *regula falsi* solution of the nonlinear algebraic equation resulting from the finite difference equivalent of Equation 11 implicit in η, at $\eta = 0$ [19].

A grid of $N\xi = 100 \times N\eta = 300$ points and a time increment $\Delta\tau = 5 \times 10^{-7}$ were found to give convergence to three significant figures in the computed steady state current for values of the dimensionless numbers DN_2 and DN_1, upto 1×10^3 and between 1×10^{-3} and 10, respectively.

The computed chronoamperometric transients are shown in Fig. 10. The transients are normalized to $I^{ss}_{DN_1 \ll 1}$, the steady state current for $DN_1 \ll 1$. Both for $DN_1 \approx 1$ and $DN_1 \ll 1$, the computed transients increase from zero to a steady state current in seconds time. The current transient for $DN_1 \approx 1$ is independent of the volume flow rate. Conversely, for $DN_1 \ll 1$ an increase in volume flow rate causes the steady state current to decrease. The steady state currents attained for $DN_1 \approx 1$ and $DN_1 \ll 1$ are in the proportion of 2 to 1.

Hence, judging from the shape of the transients and the dependency on the volume flow rate, the mechanistic scheme put forward for the oxidation of aluminium explains the transient current response of the system aluminium–electrolyte following the development of a distinct a.c. electrolytic graining morphology.

3.2.3. Comparison of computed and experimentally determined transients. From the dependence on the volume flow rate, it is evident that the transient current responses following the development of the uniform and etched-like morphology are in accordance with the current transients computed from the candidate mechanistic scheme for $DN_1 \approx 1$ and $DN_1 \ll 1$, respectively.

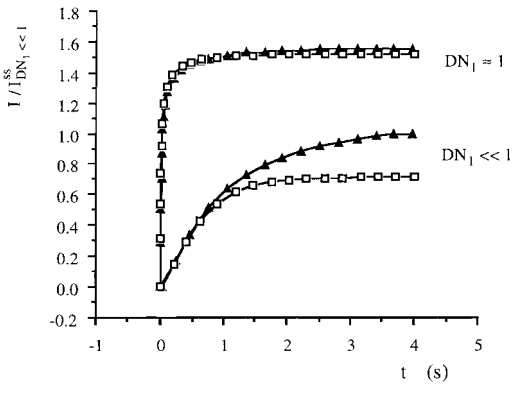

Fig. 10. Computed chronoamperometric transients. V_f: (▲) $1.7 \times 10^{-6}\,m^3\,s^{-1}$; (□) $4.3 \times 10^{-6}\,m^3\,s^{-1}$.

It is, however, to be noticed that the relative positions of the volume flow rate dependent and independent transients are inverted when the computed and the experimentally determined current responses are compared. The steady state currents computed from the candidate mechanistic scheme for $DN_1 \approx 1$ and $DN_1 \ll 1$ are in the proportion 2 to 1 (cf. Fig. 10), whereas the steady state current attained by the system aluminium–electrolyte following the development of the uniform and etched-like morphology exhibit roughly the inverse proportionality (cf. Figs 5–8). This can be explained by the fact that the transient current response is not only determined by the kinetics of the oxidation of aluminium, but also by the active surface area (cf. Equation 8).

The current transients derived from the candidate mechanistic scheme are, however, computed for a surface area independent of the graining morphology and equal to the impinged electrode surface area. Hence, the factor of about four between the computed and experimentally determined steady state currents for the oxidation of aluminium in the development of the etched-like morphology, relative to the steady state current attained in the development of the uniform morphology, indicates that the ratio of the active surface area between the etched-like and uniform morphology is about 4. This is in agreement with the ratio of the surface areas of both characteristic morphologies [14].

Considering the kinetics of the oxidation of aluminium, for $DN_2 \gg 1$ and $DN_1 \ll 1$, the dissolution rate of $Al(Cl)_3$ is high in comparison to the mass transport rate of the Cl^- ions, yet the consumption rate of Cl^- ions is low. Therefore, Cl^- ions accumulate at the electrode surface. An increase in volume flow rate reduces the amount of Cl^- ions at the electrode surface. Therefore, the oxidation rate of aluminium and hence the electrode current at any instant decrease. If $DN_1 \approx 1$, the increased formation rate of $Al(Cl)_3$ prevents the Cl^- ion concentration at the electrode surface from accumulating. The volume flow rate will therefore not affect the oxidation rate of Al. The cubic dependence of the formation rate of $Al(Cl)_3$ on the Cl^- ion concentration in the accumulation rate of Cl^- ions at the electrode surface is important.

The oxidation of aluminium is thus governed by the accumulation and, hence, by the excess of Cl^- ions at the electrode surface with respect to the bulk concentration. Whether or not the Cl^- ion concentration at the electrode surface is in excess of the bulk concentration, is determined by the ratio between the rate constant for the formation of $Al(Cl)_3$, set by the potential available at the electrode surface and the mass transport rate of the Cl^- ions.

The transient current responses subsequent to the development of the uniform and etched-like morphology being in accordance with the computed current transients for $DN_1 \approx 1$ and $DN_1 \ll 1$, respectively, indicates that the potential available for the oxidation of aluminium in the development of the

uniform morphology exceeds the potential available in the development of the etched-like morphology. This can be explained by the amount of aluminium hydroxide precipitated in the development of the etched-like morphology being larger [7, 14], producing an increased voltage drop across the layer of etch products.

3.3. *Cathodic polarization*

The transient current responses subsequent to the development of the uniform and etched-like morphology are, taking account of the reproducibility, independent of the applied potential and the volume flow rate, as well as of the a.c. electrolytic graining morphology developed. A typical example of the transient current response is shown in Fig. 11, the potential being stepped 200 mV cathodically of E_{gr}, subsequent to the a.c. electrolytic graining in the 0.20 M hydrochloric acid solution at low volume flow rate.

Starting from zero, the current reaches a maximum in a very short time. After the maximum, the current declines asymptotically to a fluctuating steady state current. The steady state current is attained in milliseconds. A poor signal to noise ratio is evident. The relative magnitude of the fluctuations is of the order of 30 to 50% of the corresponding geometrical mean value. The variance between the geometrical mean values recorded for a single experiment is in the order of 1×10^{-3} to 2×10^{-3} A.

Although appearing to be independent of the volume flow rate, taking account of the variance between recordings and the fluctuations of the steady state currents, the shape of the transient current responses indicates, that hydrogen evolution is mass transport controlled. At first the H^+ ions neighbouring the electrode surface are reduced to form hydrogen, giving a very large current. Subsequently, if the reaction is governed by mass transport, current flows only because the reduction creates a concentration gradient and hence a net flux of H^+ ions to the electrode surface, the continued flux causing the zone of depletion of H^+ ions to thicken. Therefore, the slope of the concentration profile at the electrode surface declines with time and so does the current.

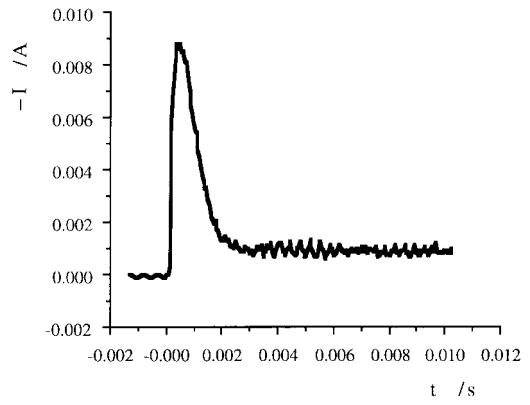

Fig. 11. Cathodic potentiostatic transient behaviour. [HCl] = 0.20 M; $E - E_{gr} = -200$ mV; $V_f = 1.7 \times 10^{-6}$ m^3 s^{-1}.

Given the time scale of milliseconds, the asymptotically decaying current cannot be mistaken for the current due to charging of the electrode–solution interface, which has been shown to be completed in tens of microseconds. The hydrogen evolution occurring during the development of both the characteristic uniform and etched-like morphology is therefore taken to be mass transport controlled.

3.4. *Mechanism of the a.c. electrolytic graining*

Under alternating current, the substrate is, in turn, anodically and cathodically polarized. At the onset of treatment, the aluminium surface is covered with a natural oxide film containing flaws, which expose the bare metal to the hydrochloric acid solution. In the absence of aggressive anions, the flaws quickly repair by forming oxide. With Cl^- ions present, pitting occurs in competition with the repair process, by active dissolution of the bare aluminium according to

$$\begin{aligned} Al + 3\,Cl &\xrightarrow{k_1} Al(Cl)_3 + 3e^- \\ Al(Cl)_3 &\xrightarrow{k_2} Al^{3+} + 3\,Cl^- \end{aligned} \qquad (9)$$

In this scheme, step 1 is rate determining. This means that once $Al(Cl)_3$ is formed, it dissolves readily not developing into an aluminium chloride film.

Initially, the number of flaws developing into pits is proportional to the bulk Cl^- ion concentration. Therefore, the charge flux across the electrode–solution interface per unit surface area taking part in the active dissolution of aluminium, decreases with increasing hydrochloric acid concentration, as does the potential available for the oxidation of aluminium. At low potential, the rate of formation of $Al(Cl)_3$, and hence the consumption of Cl^- ions, is low in comparison to the mass transport rate of Cl^-. Therefore, Cl^- is accumulated at the electrode surface, causing the number of flaws developing into pits to increase. At high potential, the increased formation rate of $Al(Cl)_3$ prevents the Cl^- ion concentration at the electrode surface from accumulating, hence reducing the number of flaws developing into pits.

With increasing treatment time or charge density imposed, at high hydrochloric acid concentration, the whole of the electrode surface is quickly activated and pitted. Conversely, at low hydrochloric acid concentration, certain preferred sites grow rapidly to form large compound pits. The adjoining surface areas remain relatively unchanged until such areas are invaded by the highly active and rapidly growing pit sites. The key factor in the development of the morphology is the accumulation of Cl^- at the electrode surface. When an excess of Cl^- is present, hemispherical pits are created. In the opposite case, an etch like morphology is formed.

The reduction of H^+ ions in the cathodic half period of the applied alternating current is mass transport controlled. The concomitant rise in interfacial

pH causes Al^{3+} ions, formed in the preceding anodic half period and not yet removed from the electrode–solution interface, to precipitate as aluminium hydroxide, as soon as the interfacial pH rises above 5.

With increasing treatment time, an aluminium hydroxide film is thus developed over the electrode surface which, in turn, reduces the potential available at the bare metal surface, both for hydrogen evolution and more important for aluminium oxidation. In order to calculate the amount of aluminium hydroxide formed, it is necessary to know the current density. This requires an estimation of the active electrode surface area during cathodic polarization, which is not possible.

From the time scale of the transient current responses for the hydrogen evolution it is apparent that the time necessary for the interfacial pH to exceed 5 is small in comparison to the cathodic half-cycle time of the applied alternating current. Moreover, the transient current responses are independent of the surface morphology developed. The interfacial concentration of Al^{3+} ions declines with time in proportion to the charge at the electrode–solution interface per unit surface area taking part in the active dissolution of aluminium. Consequently, the amount of aluminium hydroxide precipitated in the development of the etched-like morphology must be large in comparison to the amount precipitated in the development of the uniform and nonuniform morphology.

4. Conclusions

In this paper two important aspects of the a.c. electrolytic graining of aluminium in hydrochloric acid were revealed: (i) the final graining morphology is imposed by the oxidation mechanism of aluminium and (ii) an aluminium hydroxide film is formed as a result of the reduction of H^+.

The proposed mechanism for the aluminium oxidation is:

$$Al + 3\,Cl \xrightarrow{k_1} Al(Cl)_3 + 3e^-$$

$$Al(Cl)_3 \xrightarrow{k_2} Al^{3+} + 3Cl^-$$

As the first step is rate determining no solid $Al(Cl)_3$ is formed and thus no deposition of etch products occurs during the anodic half period. Due to pH changes in the cathodic half period an aluminium hydroxide etch film is deposited.

The accumulation of Cl^- at the electrode surface during the anodic half period is decisive for the characteristic graining morphology. The accumulation is governed by the ratio between the rate constant for the formation of $Al(Cl)_3$ and the mass transport rate for Cl^-. Hemispherical pits, characteristic for the uniform and non uniform morphology, are created at high Cl^- concentrations at the electrode surface. In the opposite case, an etch like morphology is formed.

The reduction of H^+ during the cathodic half period, which is mass transport controlled, leads to the deposition of $Al(OH)_3$ in the form of an etch film.

Acknowledgements

The authors thank M. Raes for the experimental work performed. The financial support of P. Laevers by I. W. T. (Vlaams Instituut voor de Bevordering van het Wetenschappelijk-Technologisch Onderzoek in de Industrie) is gratefully acknowledged.

References

[1] H. Terryn, J. Vereecken and G. E. Thompson, *Trans. Inst. Metal Finish.* **66** (1988) 116.
[2] *Idem*, *Corros. Sci.* **32** (1991) 1159.
[3] *Idem*, *ibid.* **32** (1991) 1173.
[4] P. Laevers, H. Terryn and J. Vereecken, *Trans. Inst. Metal Finish.* **70** (1992) 105.
[5] P. Laevers, H. Terryn, J. Vereecken and G. E. Thompson, *Corros. Sci.* **35** (1993) 231.
[6] P. Laevers, H. Terryn, J. Vereecken, B. Kernig and B. Grzemba, *ibid.* **38** (1996) 1.
[7] P. Laevers, 'Study of the Mechanism of the A.C. Electrolytic graining of Aluminium', PhD thesis, Vrije Universiteit Brussel, Brussels (1996).
[8] P. Laevers, A. Hubin, H. Terryn and J. Vereecken, *J. Appl. Electrochem.* **25** (1995) 1017.
[9] *Idem*, *ibid.* **25** (1995) 1023.
[10] A. J. Bard and L. R. Faulkner, 'Electrochemical Methods', J. Wiley & Sons, New York (1980).
[11] J. S. Newman, 'Electrochemical Systems', Prentice Hall, Englewood Cliffs, NJ (1991).
[12] H. Terryn, 'Electrochemical Investigation of a.c. Electrograining of Aluminium and its Porous Anodic Oxidation', PhD thesis, Vrije Universiteit Brussel, Brussels (1987).
[13] H. Terryn, J. Vereecken and N. De Jaeger, Coll. Surf. A: *Fysicochem. & Engng Asp.* **80** (1993) 171.
[14] B. Kernig, B. Grzemba and G. Scharf, *Trans. Inst. Metal Finish.* **70** (1992) 111.
[15] J. A. Richardson and G. C. Wood, *Corros. Sci.* **10** (1970) 313.
[16] G. C. Wood, W. H. Sutton, J. A. Richardson, T. N. K. Riley and A. G. Malherbe, 'The Mechanism of Pitting of Aluminium and its Alloys', Localized Corrosion NACE3 (edited by R. Sthaele, B. Brown, J. Kruger and A. Agrawal), National Association of Corrosion Engineers, Houston (1974).
[17] G. E. Thompson and G. C. Wood, *Corros. Sci.* **18** (1978) 721.
[18] N. Ibl, Fundamentals of Transport Phenomena in Electrolytic Systems, in Comprehensive Treatise of Electrochemistry,' Vol. 6 (edited by J. O'M Bockris, E. Yeager, B. E. Conway and S. Sarangapani), Plenum Press, New York (1983).
[19] D. U. von Rosenberg, 'Methods for the Solution of Practical Differential Equations', Modern Analytical and Computational Methods in Science and Mathematics (edited by R. Bellman), Elsevier, Oxford (1986).